Contribution from the Chemistry Department,
University of Houston, Houston, Texas 77204-5641

ETC Catalysis in the Electrochemical Deligation of Bis(arene)iron(II) Dications. Application of Pulse Voltammetric Techniques as a Mechanistic Tool

Z. J. Karpinski† and J. K Kochi*

Received February 13, 1992

Electron-transfer chain (ETC) catalysis in the facile electroreductive deligation of a series of bis(arene)iron(II) dications is established by the application of normal pulse (NP) and reverse pulse (RP) voltammetry in acetonitrile solution.

Introduction

Electrochemical methodology and transient techniques offer potentially valuable tools that are readily accessible for the study of inorganic and organometallic reactions—especially those in which one or more unstable or metastable intermediates are involved.[1,2] We recently showed how the combination of steady-state (bulk) electrolysis and cyclic voltammetry (CV) could be used to identify a novel catalytic process for the facile deligation of a series of bis(arene)iron(II) dications in acetonitrile solution, i.e.

$$Ar_2Fe^{2+} \xrightarrow[CH_3CN]{} 2Ar + Fe(NCCH_3)_6^{2+} \qquad (1)$$

where Ar = hexamethylbenzene (HMB), durene (DUR), mesitylene (MES), and related aromatic (arene) ligands.[3] Thus coulometry of various Ar_2Fe^{2+} complexes revealed high cathodic current efficiencies that were far in excess of unity to establish the electrocatalytic nature of the deligation in eq 1. Moreover, cyclic voltammetry identified the reduced 19-electron monocation Ar_2Fe^+ as a critical, labile intermediate, i.e.

$$Ar_2Fe^{+} \xrightarrow[CH_3CN]{} 2Ar + Fe(NCCH_3)_6^{+}, \text{ etc.} \qquad (2)$$

with lifetimes that varied with the arene donicity in the order Ar = HMB > DUR > MES. We also concluded that the follow-up reactions of the (putative) iron(I) intermediate $Fe(NCCH_3)_6^+$ formed in the deligation step (eq 2) must involve a subsequent rapid oxidation to $Fe(NCCH_3)_6^{2+}$ in order to accord with the stoichiometry of the catalytic deligation (eq 1). However, detailed CV analyses could not resolve the question as to whether $Fe(NCCH_3)_6^+$ was oxidized (a) heterogeneously at the platinum electrode or (b) homogeneously by the extant Ar_2Fe^{2+} that is relevant to electrocatalysis by the overall ECE or HOMO pathway, respectively.[3] Since this mechanistic ambiguity is intrinsic to all electrochemical studies of electron-transfer chain (ETC) catalysts,[4-6] we describe here the prototypical application of pulse voltammetric (PV) techniques[7] for the delineation of ECE and HOMO mechanisms in the catalytic deligation of bis(arene)-iron(II) complexes. In particular, we have focused on normal pulse (NP) and reverse pulse (RP) voltammetry, since they combine the advantages of double-potential-step chronoamperometry and cyclic voltammetry.[8,9] Most importantly, NP and RP voltammograms permit the separate identification of diffusion effects, heterogeneous charge-transfer kinetics, and homogeneous chemical reactions,[10-12] which is requisite for such a mechanistic differentiation. In order to briefly acquaint the uninitiated reader, the sequence in the pulse train is[13]

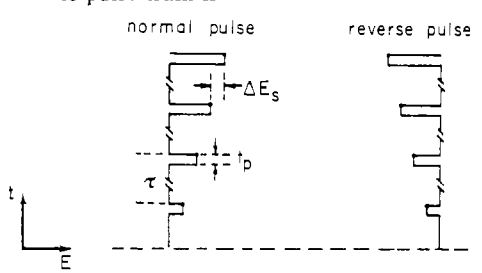

These pulse voltammetric experiments provide the chronoamperometric responses to potential pulse that are independent of the potential-time history of previous pulses. In diagram I, E_i

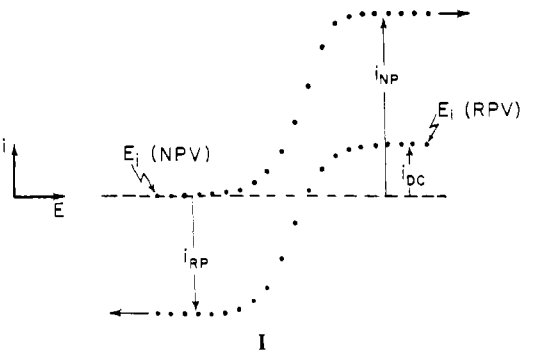

I

represents the starting potential (note left for NP and right for RP) and the current (i_{NP}, i_{DC}, or i_{RP}) sampled at the end of the pulse is directly related to the (net) concentration of the electroactive species at that potential.[10,11] For redox systems with products stable on the time scale of the experiment [i.e., τ equal to the sum of the generation time (t_g) and pulse width (t_p)], the limiting current (i_{NP}) for NP voltammetry is equal to the total wave height ($i_{DC} - i_{RP}$) in RP voltammetry.[10]

Results

The pulse voltammetric study of the electrocatalytic deligation of bis(arene)iron dications in acetonitrile at 25 °C was considerably facilitated by the highly differentiated lifetimes of the monocation Ar_2Fe^+ and the neutral species Ar_2Fe^0 as modulated by the donor strength of the arene ligands. We accordingly exploited these differences by first examining the temporal characteristics of the electron-rich $(HMB)_2Fe^{2+}$ ion in pulse voltammetry in the light

† Permanent address: Department of Chemistry, University of Warsaw, Pasteura, 1PL-02093 Warsaw, Poland.

(1) Parker, V. D. In *Topics in Organic Electrochemistry*; Fry, A. J., Britton, W. E., Eds.; Plenum Press: New York, 1986; Chapter 2.
(2) Andrieux, C. P.; Hapiot, P.; Saveant, J. M. *Chem. Rev.* **1990**, *90*, 723.
(3) Karpinski, Z. J.; Kochi, J. K. *J. Organomet. Chem.*, in press.
(4) Feldberg, S. W.; Jeftic, L. *J. Phys. Chem.* **1972**, *76*, 2439.
(5) Zizelman, P. M.; Amatore, C.; Kochi, J. K. *J. Am. Chem. Soc.* **1984**, *106*, 3771.
(6) See also: Trogler, W. C., Ed. *Organometallic Radical Processes*; Elsevier: New York, 1990.
(7) Osteryoung, J.; Schreiner, M. M. *Crit. Rev. Anal. Chem.* **1988**, *18*, S1.
(8) Galus, Z. *Fundamentals of Electrochemical Analysis*; Ellis Harwood: Chichester, U.K., 1976.
(9) Bard, A. J.; Faulkner, L. R. *Electrochemical Methods*; Wiley: New York, 1980.
(10) Osteryoung, J.; Kirowa-Eisner, E. *Anal. Chem.* **1980**, *52*, 62.
(11) (a) Osteryoung, J.; Talmor, D.; Hermolin, J.; Kirowa-Eisner, E. *J. Phys. Chem.* **1981**, *85*, 285. (b) Kashti-Kaplan, S.; Hermolin, J.; Kirowa-Eisner, E. *J. Electrochem. Soc.* **1981**, *128*, 802.
(12) Karpinski, Z. J. *Bioelectrochem. Bioenerg.* **1989**, *21*, 261.
(13) In practice (see Experimental Section), the equilibration period t_d preceded each pulse sequence (see refs 14 and 15), but for clarity is omitted in diagram I.
(14) (a) Karpinski, Z. J.; Osteryoung, R. A. *J. Electroanal. Chem. Interfacial Electrochem.* **1984**, *164*, 281. (b) Karpinski, Z. J. *Anal. Chem.* **1986**, *58*, 2099.
(15) Karpinski, Z. J.; Osteryoung, R. A. *J. Electroanal. Chem. Interfacial Electrochem.* **1991**, *307*, 47.

0020-1669/92/1331-2762$03.00/0

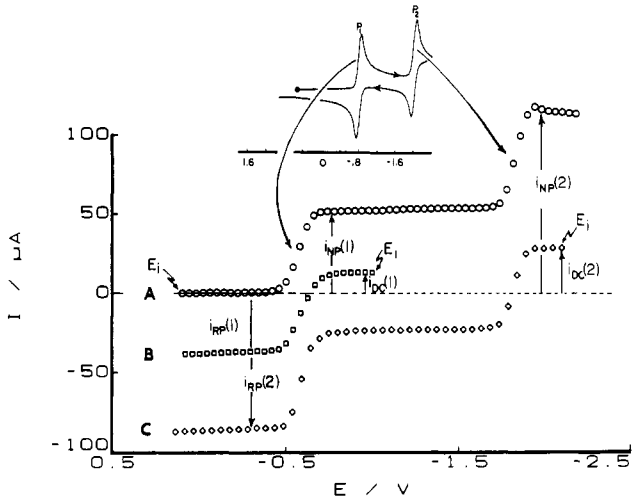

Figure 1. Normal pulse (A) and reverse pulse (B, C) voltammograms (with t_p = 20 ms and τ = 250 ms) of 1.9 mM $(HMB)_2Fe^{2+}$ in acetonitrile containing 0.1 M TBAH at 256 K. The inset shows the initial negative-scan cyclic voltammogram at v = 0.5 V s^{-1} to identify the cathodic waves P_1 and P_2 for $(HMB)_2Fe^{2+}$ and $(HMB)_2Fe^{+}$, respectively.

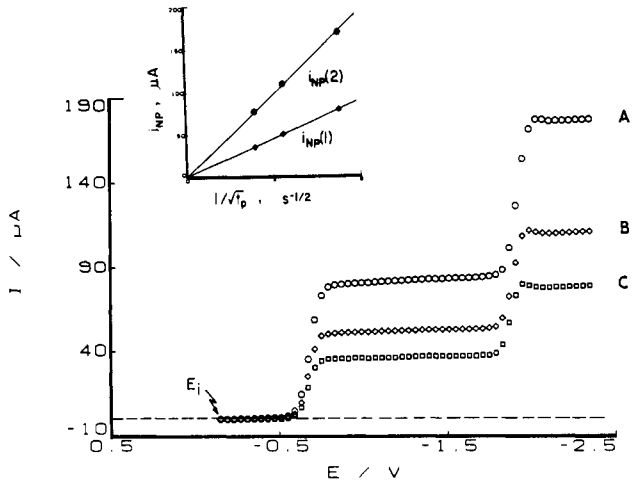

Figure 2. Normal pulse voltammograms with t_p = 20 (A), 50 (B), and 100 ms (C) for 2.2 mM $(HMB)_2Fe^{2+}$ in acetonitrile at 298 K. The inset shows the variations of the limiting currents $i_{NP}(1)$ and $i_{NP}(2)$ with the pulse widths $(t_p^{-1/2})$.

of its reversible CV behavior and then extending the pulse voltammetry to the progressively more labile intermediates derived from $(DUR)_2Fe^{2+}$ and $(MES)_2Fe^{2+}$ in the following manner.

I. Pulse Voltammetry of Bis(hexamethylbenzene)iron(II). The bis(hexamethylbenzene)iron dication, $(HMB)_2Fe^{2+}$, is subject to the stepwise reduction at the reversible potentials of $E_1° = -0.68$ V and $E_2° = -1.87$ V to afford the rather persistent (19-electron) monocation and the neutral (20-electron) species, respectively, as indicated by the reversible CV behavior of the cathodic peaks P_1 and P_2 even at slow scan rates (v > 0.5 V s^{-1}).[3]

$$(HMB)_2Fe^{2+} \overset{P_1}{\rightleftharpoons} (HMB)_2Fe^{+} \overset{P_2}{\rightleftharpoons} (HMB)_2Fe^{0} \qquad (3)$$

The corresponding normal pulse (NP) voltammogram of $(HMB)_2Fe^{2+}$ commencing at $E_i = -0.2$ V is presented in Figure 1A with the limiting current $i_{NP}(1)$ for $(HMB)_2Fe^{+}$ equal to half the limiting current $i_{NP}(2)$ for $(HMB)_2Fe^{0}$ at the half-wave potentials of P_1 and P_2, respectively. [Compare with the initial negative-scan cyclic voltammogram of $(HMB)_2Fe^{2+}$ shown in the inset.] Importantly, the reverse pulse (RP) voltammograms B and C commencing at −1.0 and −2.1 V, respectively, showed the total wave heights ($i_{DC} - i_{RP}$) equal to the NP wave heights (i_{NP}). The latter thus established the two-step reduction in eq 3 that was unaffected by any (fast) transformation of either $(HMB)_2Fe^{+}$ or $(HMB)_2Fe^{0}$. Furthermore, the variation of the NP voltammogram of $(HMB)_2Fe^{2+}$ with the pulse width (t_p) in Figure 2 (inset)

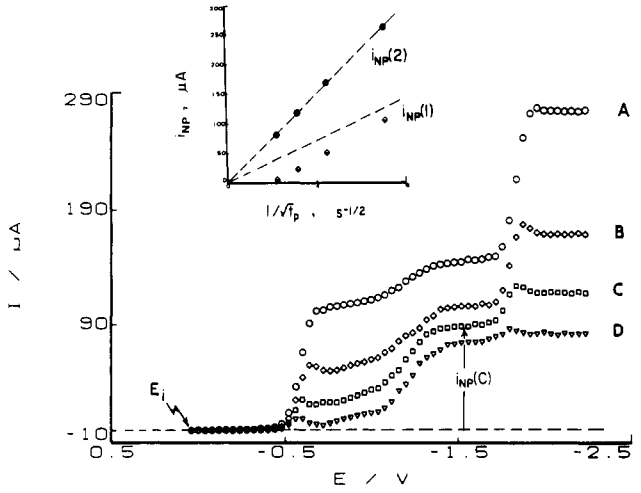

Figure 3. Normal pulse voltammograms with t_p = 20 (A), 50 (B), 100 (C), and 200 ms (D) for 3.5 mM $(DUR)_2Fe^{2+}$ in acetonitrile at 298 K. The inset shows the correlation of $i_{NP}(1)$ and $i_{NP}(2)$ versus $t_p^{-1/2}$. (The dashed lines represent the expected linear trend for the diffusion-controlled current.)

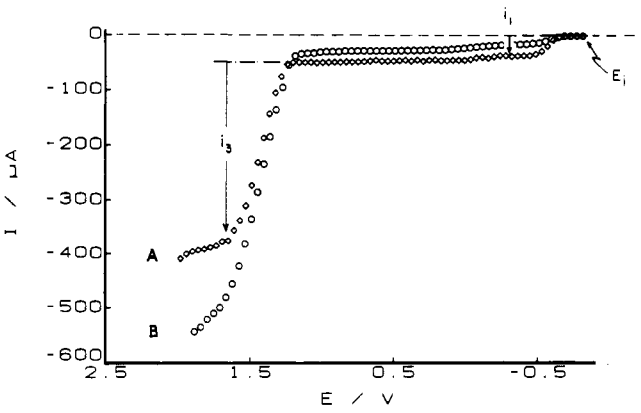

Figure 4. Reverse pulse voltammograms with τ = 0.25 (A) and 0.50 s (B) at t_p = 20 ms for 3.5 mM $(DUR)_2Fe^{2+}$ in acetonitrile at 298 K.

indicated that the microelectrolysis current sampled after 20, 50, and 100 ms increased linearly with the reciprocal of square root of time at all potentials, as expected for a diffusion-controlled current. The latter condition was also obeyed by the currents produced on the rising portions of the NP waves so that their half-wave potentials were more or less independent of the pulse times. Together they showed that the heterogeneous electron-transfer steps for the successive reduction of $(HMB)_2Fe^{2+}$ were fast on the millisecond time scale, and thus P_1 and P_2 were reversible at 25 °C (eq 3).[10,16]

II. Pulse Voltammetry of Bis(durene)iron(II). The bis(durene)iron dication upon reduction afforded highly transient intermediates, as indicated by the (chemically) reversible cyclic voltammograms that were achieved only at fast scan rates (v > 200 V s^{-1}).[3] Likewise, the normal pulse voltammogram of $(DUR)_2Fe^{2+}$ generally resembled that of $(HMB)_2Fe^{2+}$ only at the shortest pulse width of t_p = 20 ms, as deduced from the magnitudes of the limiting currents in Figure 3A for the corresponding pair of redox couples, i.e.

$$(DUR)_2Fe^{+} \overset{P_1}{\rightleftharpoons} (DUR)_2Fe^{+} \overset{P_2}{\rightleftharpoons} (DUR)_2Fe^{0} \qquad (4)$$

Lengthening of the pulse width to t_p = 50 ms (B), 100 ms (C), and 200 ms (D) was accompanied by a dramatic decrease of the limiting currents for waves P_1 and P_2 that was accompanied by the concomitant growth (at potentials of ca. −1.20 V) of a new wave PC from the ferrous ion $Fe(NCCH_3)_6^{2+}$. Since the latter was associated with the deligation of the monocation (see eq 2),

(16) Oldham, K. B.; Parry, E. P. *Anal. Chem.* **1968**, *40*, 65; **1970**, *42*, 229.

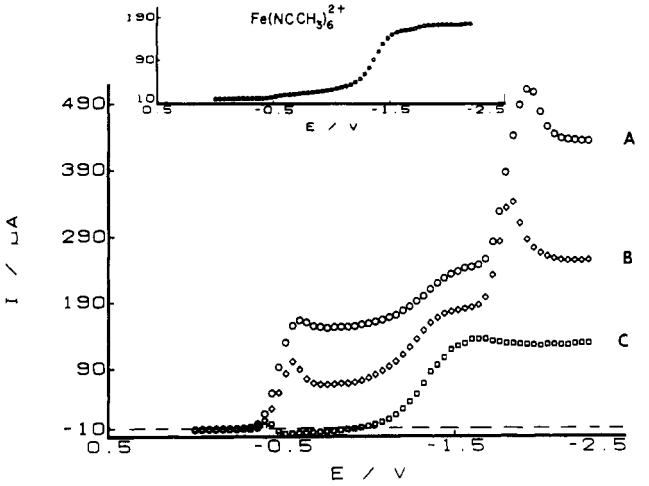

Figure 5. Normal pulse voltammograms with t_p = 20 (A), 50 (B), and 100 ms (C) for 4.0 mM $(MES)_2Fe^{2+}$ in acetonitrile at 298 K. The inset shows the NPV (t_p = 20 ms and τ = 5 s) for 3.0 mM $Fe(NCCH_3)_6^{2+}$ in acetonitrile at 298 K.

the time-dependent changes in Figure 3 largely reflected the kinetics of eq 5. Most importantly, the reverse pulse voltammetry

$$(DUR)_2Fe^+ \rightarrow 2DUR + Fe(NCCH_3)_6^+ \qquad (5)$$

of $(DUR)_2Fe^{2+}$ in Figure 4 at the successively longer times of τ = 250 and 500 ms for the electroduction actually showed an *anodic* current i_{DC} of 3 μA. The latter most clearly resulted (at potentials of ca. −0.7 V) from the depletion of $(DUR)_2Fe^{2+}$ by a homogeneous process involving the product of eq 5,[17] i.e.

$$(DUR)_2Fe^{2+} + Fe(NCCH_3)_6^+ \rightarrow (DUR)_2Fe^+ + Fe(NCCH_3)_6^{2+} \qquad (6)$$

The same conclusion can be drawn from the deviation of the limiting current $i_{NP}(1)$ from the linear dependence on the square root of time ($t_p^{-1/2}$), as shown in Figure 3 (inset) by the experimental points that fell below the (dashed) line expected from a diffusion-controlled current. It is also noteworthy that the decrease of wave P_1 in Figure 4 was accompanied by a corresponding increase of the wave P_3 associated with the oxidation of the free (uncomplexed) durene. Thus, the anodic current $i_{RP}(3)$ in voltammogram B (Figure 4) was nearly 4 times larger than the cathodic current $i_{NP}(1)$ for $(DUR)_2Fe^{2+/+}$ at the same pulse width (t_p = 20 ms, see curve A in Figure 3). Such a current ratio, i.e., $i_{RP}(3)/i_{NP}(1)$, established the liberation of two arene ligands for each bis(arene)iron ion, as presented in eq 5.[18]

III. Pulse Voltammetry of Bis(mesitylene)iron(II). The apparently complex pulse voltammetric behavior of $(MES)_2Fe^{2+}$ in Figure 5 can be deciphered, if it is considered as the ultimate outgrowth of $(HMB)_2Fe^{2+}$ and $(DUR)_2Fe^{2+}$, as presented above. Thus the highly transient monocation $(MES)_2Fe^+$ is evident by the very rapid diminution of the limiting current $i_{NP}(1)$ with increasing pulse widths—until it actually resulted in an *anodic* current at t_p = 200 ms, while wave C totally replaced wave P_2 [compare curve C in Figure 5 with curve D for $(DUR)_2Fe^{2+}$ in Figure 3 and curve C for $(HMB)_2Fe^{2+}$ in Figure 2].[19] Thus, the NPV experiments showed that, after 200 ms, the electroreduction

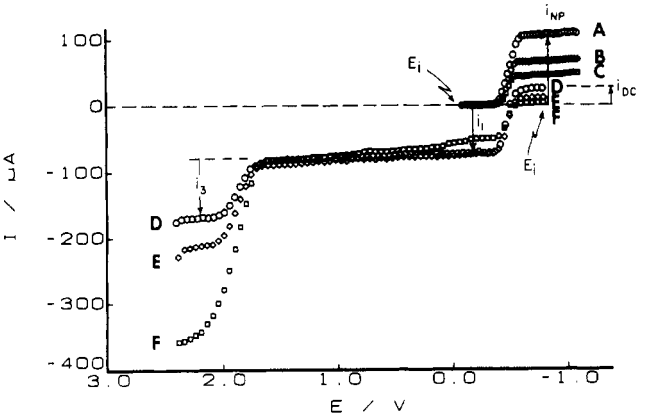

Figure 6. Normal pulse (A, B, C) and reverse pulse (D, E, F) voltammograms with t_p = 20 (A, D, E, F), 50 (B), and 100 ms (C) at τ = 0.25 (D), 0.5 (E), and 2.0 s (F) for 5.0 mM $(MES)_2Fe^{2+}$ at 256 K.

of $(MES)_2Fe^{2+}$ was complete and only products like those in reactions 5 and 6 were detected. The anodic current in curve C (Figure 5) returned to zero at potential <−0.9 V. A similar small increase of the current at the same potential was noticed in the NP voltammograms for $(DUR)_2Fe^{2+}$ (curves C and D in Figure 3), indicating that the oxidation of $Fe(NCCH_3)_6^+$ ceased at potentials more negative than −0.9 V.

IV. Temperature Dependence in the Pulse Voltammetry of Bis(arene)iron(II). The pulse voltammetry of $(DUR)_2Fe^{2+}$ and $(MES)_2Fe^{2+}$ was examined in the temperature range between 256 and 298 K to extend the kinetics range for the electrogenerated monocations $(DUR)_2Fe^+$ and $(MES)_2Fe^+$. The time dependence of the limiting currents in wave P_1 was studied in normal pulse experiments at pulse widths that varied from t_p = 20 to 100 ms, while the changes in the concentrations of the monocations (P_1) and free arenes (P_3) after generation steps of t_g = 230, 480, and 1980 ms[20] were monitored in reverse pulse experiments. The experimental current ratios, typically obtained from voltammograms such as those illustrated in Figure 6, are listed in Table I. [For the current designations of $(i_{DC} - i_1)$, $-i_3$, and i_{DC}, see the labeling in Figure 6.]

Discussion

Pulse voltammetric studies of the electrocatalytic deligation of bis(arene)iron dications clearly identify the difference between the well-behaved, reversible redox couples for $(HMB)_2Fe^{2+}$ in eq 3 and the facile decomposition accompanying the reduction of $(DUR)_2Fe^{2+}$ (eq 5) and $(MES)_2Fe^{2+}$. With the latter, reverse pulse voltammetry enables the simultaneous monitoring of the decomposition of the monocation [$(DUR)_2Fe^+$ or $(MES)_2Fe^+$] and the formation of free arene (DUR, MES). Thus, at increasingly prolonged generation times in the RPV experiments shown in Figures 4 and 6, the total wave height $(i_{DC} - i_1)$ of P_1 for $(DUR)_2Fe^+$ or $(MES)_2Fe^+$ decreases concomitantly with the growth of wave P_3 ($i_3/4$) of the liberated DUR or MES. The comparison of wave heights (concentration) established the (stoichiometric) relationship $i_{NP}(1) = i_3/4$ for the formation of two free arenes for each Ar_2Fe^+ consumed on the millisecond time scale of the transient experiment. Furthermore, the decrease in the limiting current for wave P_1 is accompanied by the appearance of wave P_C for $Fe(NCCH_3)_6^{2+}$ arising from a homogeneous oxidation according to eq 6.[23] Accordingly, the pertinent redox steps to be included in the mechanisms for the electrocatalytic deligation of bis(arene)iron dications are as follows:

(17) The diminution of P_1 can result from an algebraic summation of currents due to the reduction of Ar_2Fe^{2+} (cathodic) and the oxidation of $Fe(NCCH_3)_6^+$ (anodic). However, when the reaction in eq 6 is relatively slow, the current cannot decay below zero.

(18) For 2-electron arene oxidation in acetonitrile, see: Bewick, A.; Mellor, J. M.; Pons, B. S. *Electrochim. Acta* **1980**, *25*, 931.

(19) Maxima in the NP limiting current, such as $i_{NP}(2)$ for P_3 (see curves A and B in Figure 5), are usually attributed to adsorption of the reactant at the electrode surface.[20] Other likely reasons for the current maxima are convection effects caused by simultaneous iron deposition and the formation of Ar_2Fe^0, together with instrumental artifacts due to limited current handling capabilities of the potentiostat which could not be prevented.

(20) Barker, G. C.; Bolzan, J. A. *Z. Anal. Chem.* **1966**, 216, 215.

(21) Lovric, M. *J. Electroanal. Chem. Interfacial Electrochem.* **1984**, *170*, 143.

(22) Note that the generation time $t_g = \tau - t_p$ in diagram I.

(23) In PV, a competitive pathway for the formation of $Fe(NCCH_3)_6^{2+}$ via the oxidation of $Fe(NCCH_3)_6^+$ as described in eq 9 cannot proceed at the potentials of iron deposition (i.e., at electrode potentials more negative than −1.1 V). The contribution from eq 9 can be obtained in the CV experiment by scanning between waves P_1 and C.

$$Ar_2Fe^{2+} + e \rightleftharpoons Ar_2Fe^{+} \quad (7)$$

$$Ar_2Fe^{+} \xrightarrow[CH_3CN]{k_1} 2Ar + Fe(NCCH_3)_6^{+} \quad (8)$$

$$Fe(NCCH_3)_6^{+} \rightleftharpoons Fe(NCCH_3)_6^{2+} + e \quad (9)$$

$$Fe(NCCH_3)_6^{+} + Ar_2Fe^{2+} \rightleftharpoons Fe(NCCH_3)_6^{2+} + Ar_2Fe^{+} \quad (10)$$

The combination of eqs 7–9 represents the classical electrochemical ECE pathway in which the oxidation of the product of the chemical reaction $Fe(NCCH_3)_6^{+}$ at the electrode completes the electrocatalysis.[4] The alternative combination of eqs 7–10 has been identified in homogeneous electron-transfer contributions to electrochemical mechanisms,[4,24] and it corresponds to EC-HOMO or is referred to simply as HOMO.[5] More generally, the combination of eqs 7, 8, and 10 has been used to describe various chain mechanisms for ligand substitutions carried out thermally, and it is usually referred to as electron-transfer chain (ECT) catalysis.[25,26] In the electrochemical HOMO and thermal ETC processes, the rapidity of the redox equilibrium in eq 10 propagates the chain catalytic mechanism. Compelling evidence for such a homogeneous electron transfer during the electrocatalytic deligation is provided by the pulse voltammetric technique. Thus in the NP experiment, the limiting current for the reduction of Ar_2Fe^{2+} actually changes sign at longer pulse times (t_p), as shown by the observation of anodic currents[27] for $i_{NP}(1)$ and i_{DC} in curves C and B in Figures 5 and 4, respectively (see also Table I). Moreover, the limiting current for the first anodic wave (i_1) in the RP experiment decreases to a value below the minimum current for the ECE process, as shown by voltammogram B in Figure 4.[27] Most importantly, the variation of the limiting current $i_{NP}(1)$ with increasing pulse times can be compared with the chronoamperometric response (i_{NP}^{d}) simulated on the basis of either eq 9 (ECE) or eq 10 (HOMO), and the first-order rate constant k_1 for the deligation step in eq 8 can be obtained, as described in the Experimental Section. Such an analysis of NVP currents is equivalent to the scan-rate dependence of CV peak currents[4,5] or single-step chronoamperometry,[4] both of which have been previously employed in the kinetics analysis of ETC ligand substitution. The comparative results, listed in Table II as normalized limiting current ratios, favor the HOMO mechanism from the electrocatalytic deligation for both $(DUR)_2Fe^{2+}$ and $(MES)_2Fe^{2+}$. As an independent check, a similar comparison can be carried out with the limiting current $i_{NP}(C)$ for wave P_C that represents the reduction of $Fe(NCCH_3)_6^{2+}$ (vide infra). Indeed, the detection of $Fe(NCCH_3)_6^{2+}$ in the NPV experiments at potentials where $Fe(NCCH_3)_6^{+}$ cannot be oxidized (e.g., during the potentiostatic bulk electrolysis) identifies the HOMO mechanism. Moreover, the quantitative agreement of the experimental limiting currents at P_C with those obtained in the simulation (columns 7 and 8 in Table II) shows that the homogeneous electron transfer in eq 10 is a fast equilibrium.

The working curve in Figure 7 shows how the normalized limiting current ratio varies with the normal pulse voltammetric parameter t_p and the lifetime $1/k_1$ of the monocation according to whether eq 9 (ECE) or eq 10 (HOMO) dominates. Thus, for the HOMO mechanism, the current for P_1 is predicted to decrease faster than that for the ECE mechanism and actually changes sign at values of k_1t_p greater than 2. The limiting cathodic current to become anodic is thus diagnostic of the HOMO mechanism, since i_{NP} in the ECE process can never drop below zero. The mechanistic differentiation between ECE and HOMO schemes is also delineated in reverse pulse voltammetry of the electrocatalytic deligation of $(DUR)_2Fe^{2+}$ and $(MES)_2Fe^{2+}$. Thus, the working curves based on the normalized limiting current ratios for wave P_1 and wave P_3 are shown in Figure 8, and such results of computer simulation are compared with the experimental values in Table III. The differences, which are most apparent at $k_1 \gg 1$, lead to the HOMO mechanism for electrocatalytic deligation. Indeed, all those voltammetric features alluded to earlier, such as negative NP and DC currents and the decay of the first RP wave below the limiting wave height for the ECE pathway, are observed. This evidence, together with an adherence of all the

Table I. Temperature Dependence of the Experimental Current Ratios for the Reverse Pulse Voltammetry of Bis(arene)iron(II)[a]

Ar_2Fe^{2+} Ar (mM)	T (K)	τ (s)	$(i_{DC} - i_1)/i_{NP}$	$-i_3/i_{NP}$	i_{DC}/i_{NP}
DUR (4.8)	256	0.25	0.93	0.35	0.24
		0.50	0.84	0.60	0.14
		2.0	0.63	1.6	0.04
DUR (5.2)	266	0.25	0.86	0.57	0.22
		0.50	0.76	0.90	0.12
		2.0	0.44	1.8	0.01
DUR (4.7)	271	0.25	0.77	0.90	0.16
		0.50	0.60	1.4	0.07
		2.0	0.25	2.8	−0.02
DUR (3.9)	283	0.25	0.62	1.7	0.1
		0.50	0.39	2.6	−0.02
DUR (4.1)	298	0.25	0.35	3.2	−0.04
		0.50	0.14	4.4	−0.05
MES (5.2)	256	0.25	0.87	0.71	0.22
		0.50	0.78	1.05	0.11
		2.0	0.42	2.7	0.01
MES (4.9)	266	0.25	0.80	0.90	0.17
		0.50	0.65	0.16	0.06
		2.0	0.19	3.5	−0.01
MES (4.2)	283	0.25	0.76	1.1	0.14
		0.50	0.20	3.6	−0.02
MES (4.0)	298	0.25	0.20	4.8	−0.04

[a] In acetonitrile containing 0.1 M (TBA)PF_6 at t_P = 20 ms. See Figure 6 for the current identifications.

Table II. Rate Constants for the Deligation of Ar_2Fe^{+} Based on Normal Pulse Voltammetric Current Ratios[a]

Ar_2Fe^{2+} Ar (mM)	T (K)	t_p (ms)	$i_{NP}(1)/i_{NP}^{d}$[b] exp	HOMO	ECE	$i_{NP}(C)/i_{NP}^{d}$[b] exp	HOMO	k_1 (s^{-1})
DUR (4.1)	298	20	0.84	0.85	0.85	1.16	1.16	7.5
		50	0.65	0.66	0.68	1.38	1.38	
		100	0.43	0.41	0.46	1.62	1.74	
		200	0.10	0.06	0.20	1.99	2.0	
MES (4.2)	298	20	0.76	0.77	0.78	1.25	1.24	12
		50	0.53	0.50	0.54	1.48	1.60	
		200	−0.02	−0.15	0.06	2.0	2.0	

[a] In acetonitrile containing 0.1 M (TBA)PF_6 at 25 °C. [b] i_{NP}^{d} = diffusion-controlled limiting current.

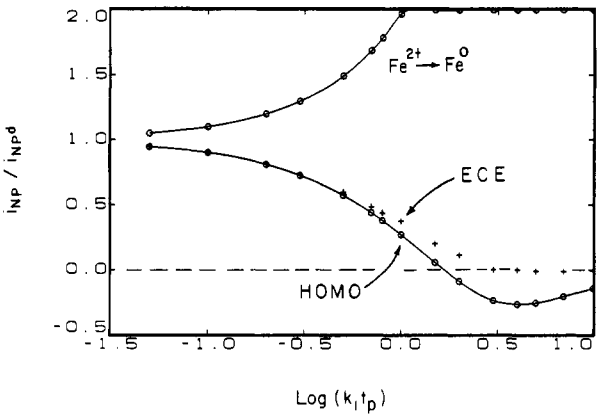

Figure 7. Computer simulation of the limiting current $i_{NP}(1)$ normalized to the diffusion-controlled value as a function of the deligation rate constant k_1 (eq 8) and the pulse width (t_p) for the ECE (+) and HOMO (O) mechanisms.

(24) Evans, D. H. *Chem. Rev.* **1990**, *90*, 739.
(25) Chanon, M. *Acc. Chem. Res.* **1987**, *20*, 214. Julliard, M.; Chanon, M. *Chem. Rev.* **1983**, *83*, 425.
(26) Hershberger, J. W.; Klingler, R. J.; Kochi, J. K. *J. Am. Chem. Soc.* **1982**, *104*, 3034; *J. Am. Chem. Soc.* **1983**, *105*, 61.
(27) Homogeneous reactions in eqs 8 and 10 lead to the appearance of an excess of $Fe(NCCH_3)_6^{+}$ (which is readily oxidized at these electrode potentials) over Ar_2Fe^{2+}. Similar chronoamperometric results were obtained by Feldberg and Jeftic in ref 4.

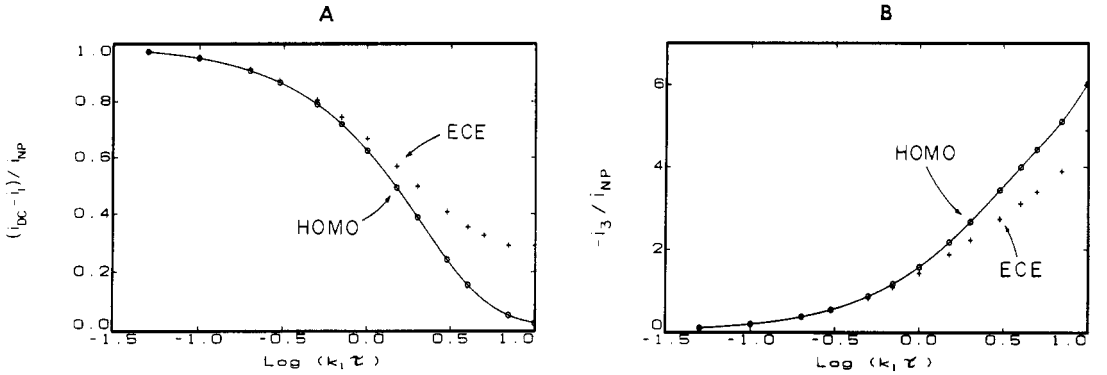

Figure 8. Calculated dependences of the RP (normalized) current ratios for (A) Ar_2Fe^{2+} and (B) free Ar on the rate constant k_1 and pulse width t_p based on the ECE (+) and HOMO (○) mechanisms.

Table III. Calculated Current Ratios (Normalized) and Rate Constants k_1 Based on the ECE and HOMO Mechanisms[a]

Ar_2Fe^{2+} Ar (mM)	T (K)	τ (s)	$(i_{DC} - i_l)/i_{NP}$		$-i_3/i_{NP}$		i_{DC}/i_{NP}		k_1 (s^{-1})
			HOMO	ECE	HOMO	ECE	HOMO	ECE	
DUR (4.8)	256	0.25	0.93	0.93	0.29	0.28	0.24	0.24	0.6
		0.50	0.87	0.87	0.54	0.52	0.15	0.15	
		2.0	0.56	0.61	1.8	1.6	0.02	0.03	
DUR (5.2)	266	0.25	0.88	0.89	0.51	0.47	0.22	0.22	1.2
		0.50	0.77	0.79	0.95	0.90	0.11	0.12	
		2.0	0.35	0.48	2.5	2.2	0.01	0.01	
DUR (4.7)	271	0.25	0.80	0.81	0.88	0.80	0.17	0.18	2.0
		0.50	0.62	0.67	1.6	1.4	0.06	0.07	
		2.0	0.15	0.32	3.5	2.9	−0.03	0.00	
DUR (3.9)	283	0.25	0.63	0.68	1.65	1.4	0.08	0.11	4.0
		0.50	0.39	0.50	2.65	2.2	−0.02	0.03	
DUR (4.1)	298	0.25	0.38	0.51	3.0	2.4	−0.03	0.03	8.5
		0.50	0.14	0.34	4.3	3.2	−0.06	0.00	
MES (5.2)	256	0.25	0.88	0.89	0.51	0.47	0.22	0.22	1.1
		0.50	0.77	0.79	0.95	0.90	0.11	0.11	
		2.0	0.35	0.45	2.7	2.3	−0.01	0.00	
MES (4.9)	266	0.25	0.80	0.82	0.85	0.77	0.17	0.18	1.9
		0.50	0.64	0.68	1.5	1.35	0.06	0.08	
		2.0	0.17	0.33	3.5	2.8	−0.02	0.00	
MES (4.2)	283	0.25	0.77	0.79	1.0	0.90	0.15	0.16	7
		0.50	0.19	0.38	3.7	2.9	−0.05	0.00	
MES (4.0)	298	0.25	0.21	0.42	4.3	3.2	−0.09	0.00	14

[a] For the experimental current ratios listed in Table I.

current ratios to the HOMO scheme, provides a more important mechanistic criterion than an agreement of any individual value of the current ratio with the simulated working curve (see Tables II and III). Finally, the dominance of the homogeneous electron transfer (eq 10) over the heterogeneous process (eq 9) agrees with an estimate of the second-order rate constant k_{HOMO} from the Marcus relationship.[28] Using the value of $E_{ox}° = -0.9$ V vs Fc for $Fe(NCCH_3)_6^+$ as indicated by NP voltammetry,[29] we calculate the value of $k_{HOMO} = 4 \times 10^3$ m^{-1} s^{-1} for $(HMB)_2Fe^{2+}$ to increase regularly to 9×10^4 and 2×10^6 m^{-1} s^{-1} for $(DUR)_2Fe^{2+}$ and $(MES)_2Fe^{2+}$, respectively.

The temperature dependence of the rate constant k_1 for the deligation step in eq 8 is shown in Figure 9. The linear Eyring plots (with $r = 0.995$) afforded values of the activation enthalpy $\Delta H^‡ = 9.1$ and 8.9 kcal mol^{-1} and entropy of activation $\Delta S^‡ = -21$ and -22 cal mol^{-1} K^{-1} for the deligation of $(DUR)_2Fe^+$ and $(MES)_2Fe^+$, respectively, in acetonitrile solution. Such negative values of the activation entropy are often ascribed to bimolecular (associative) processes[30] but may also be (partly) ascribed to the freezing of the ring rotation in the (η^6-arene)iron complex to a static η^4- or η^2-arene intermediate prior to ligand loss.[31]

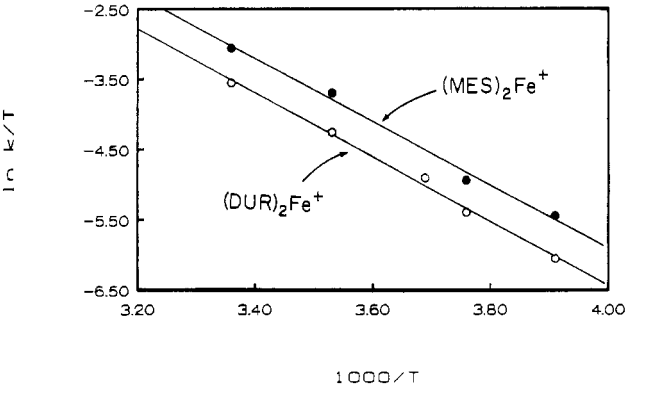

Figure 9. Temperature dependences of the deligation rate constants k_1 for $(DUR)_2Fe^+$ and $(MES)_2Fe^+$ in acetonitrile.

Experimental Section

Materials. The crystalline bis(arene)iron(II) hexafluorophosphate salts were prepared by the treatment of mesitylene or durene with anhydrous ferric chloride (Pennwalt) and aluminum chloride (Fluka) according to the literature procedure.[32,33] The hexamethylbenzene derivative $(HMB)_2Fe^{2+}(PF_6^-)_2$ was prepared from ferrous chloride, aluminum chloride, and hexamethylbenzene by an analogous procedure.[34] Tetra-

(28) Marcus, R. A. *J. Phys. Chem.* **1963**, *67*, 853.
(29) The standard heterogeneous rate constants for the reduction of Ar_2Fe^{2+} and $Fe(NCCH_3)_6^{2+}$ were taken as $k_s = 0.5$ cm^{-1} s^{-1} to represent the low-limit estimates. The values of k_{HOMO} also represent the low limits.
(30) Basolo, F.; Pearson, R. G. *Mechanism of Inorganic Reactions*; Wiley: New York, 1967.
(31) See: Ruiz, J.; Lacoste, M.; Astruc, D. *J. Am. Chem. Soc.* **1990**, *112*, 5471.
(32) Helling, J. F.; Braitsch, D. M. *J. Am. Chem. Soc.* **1970**, *92*, 7207.
(33) Helling, J. F.; Rice, S. L.; Braitsch, D. M.; Mayer, T. *J. Chem. Soc., Chem. Commun.* **1971**, 930.
(34) Mandon, D.; Astruc, D. *J. Organomet. Chem.* **1989**, *369*, 383.

n-butylammonium hexafluorophosphate (Johnson Matthey) was recrystallized from acetonitrile and dried in vacuo. Acetonitrile (HPLC grade, Fisher) was stirred for 24 h with 0.1% by weight $KMnO_4$ and then heated to boiling, cooled, and filtered from the brown MnO_2 residue. The filtered acetonitrile was distilled from P_2O_5 (2 g L^{-1}) and redistilled from CaH_2 under an atmosphere of argon.

Instrumentation. All voltammetric experiments were performed with a BAS 100B electrochemical analyzer using the conventional three-electrode arrangement. A platinum disk electrode (BAS) served as the working electrode and was referenced to Ag^+/Ag (0.01 M $AgClO_4$ and 0.1 M (TBA)PF_6 in acetonitrile) or an aqueous SCE reference electrode. Both reference electrodes were calibrated with a ferrocene standard,[35,36] and all potentials in this work are referred to the potential of Cp_2Fe. A platinum flag electrode was used as the auxiliary electrode.

Pulse Voltammetry. The potential–time waveform in normal pulse voltammetry consists of a train of potential pulses of increasing amplitude that is applied from a constant initial potential E_i. The value of E_i is chosen so no current flows (see diagram I). With the proper renewal of initial concentration conditions,[14,15] it is a simplest of all voltammetric techniques, because the chronoamperometric response to each potential pulse is independent of the potential–time history before the pulse is applied. Therefore a voltammogram with a well-defined limiting current plateau is obtained (I). The same potential–time waveform is used in reverse pulse voltammetric experiments, but the initial potential is chosen so that the reactant undergoes electrolysis at the diffusion-controlled rate. The pulses are applied in the reverse direction to elicit the current–potential curve of the charge-transfer products. When constant initial conditions are ensured for each pulse cycle,[14,15] a set of well-defined double-step chronoamperometric responses is collected over a range of potentials of interest (I). Together, the twin set of normal and reverse pulse voltammograms provides a qualitative screening over a wide potential range for the identification of electroactive species. The characteristic values of the half-wave potentials as well as quantitative featues of wave shapes reflect the heterogeneous electron-transfer kinetics and limiting currents, which are *independent* of the charge-transfer kinetics and the potential–time history of the previous pulses. The relatively slow chemical reactions in the reduction of bis(arene)iron dications required an experimental time scale of fractions of a second, without the use of very small electrodes for the renewal of the initial concentration conditions between pulses.[15] Therefore, the boundary renewal is ensured by a most convenient modification of a hydrodynamic step for an airtight cell, i.e. ca. 1 s period of stirring (t_r) of the solution at the beginning of a delay time. The stirring time and the delay time (t_d), over which the working electrode was disconnected from the potentiostat (I), were controlled by a pair of timing relays activated by the TTL signal from the BAS 100B analyzer.

Kinetic Data from Pulse Voltammetric Experiments. The most convenient method for the determination of the kinetics of a chemical reaction from pulse voltammetric data involves the analysis of the ratios of limiting currents which are independent of heterogeneous electron-transfer rates and the electrode area. For many mechanistic schemes, these are also independent of diffusion coefficients.[10] In such an analysis of the limiting current ratios, the theory of double-step chronoamperometry can be used,[8,9] and for some mechanistic schemes analytical solutions are available. However, the differential equations for double-step chronoamperometry for kinetic schemes involving solution electron-transfer reactions cannot be solved analytically. Therefore, a set of chronoamperometric responses was simulated using Feldberg's method of finite difference,[37] and the Crank–Nicholson half-implicit algorithm[38] was used to solve the diffusion equations. Two limiting kinetic situations were simulated. In the ECE mechanism, reaction 5 was the only chemical reaction considered, while in the HOMO mechanism, reaction 6 was additionally included as an equilibrium. [The simulated current ratios were independent of the equilibrium constant K_2 (eq 10) if it was larger than 1000, and the value of 10^5 was used in the simulations.] Boundary conditions for simulations of the limiting current values did not include the kinetic parameters for the heterogeneous electron-transfer steps. Therefore, the following sets of boundary conditions were used for the concentrations of Ar_2Fe^{2+}, Ar_2Fe^{+}, $Fe(NCCH_3)_6^{+}$, $Fe(NCCH_3)_6^{2+}$, and Ar which are represented below as *a*, *b*, *c*, *d*, and *e*, respectively: (1) for i_{NP} and the generation step of RP experiments (i_{DC}), $a_0 = c_0 = 0$ $(\partial a/\partial x)_0 + (\partial b/\partial x)_0 = 0$, and $(\partial c/\partial x)_0 + (\partial d/\partial x)_0 = 0$; (2) for i_{NP}^{C}, $a_0 = c_0 = d_0 = 0$ and $(\partial a/\partial x)_0 + (\partial b/\partial x)_0 = 0$; (3) for i_{RP}^{1}, $b_0 = c_0 = 0$ $(\partial a/\partial x)_0 + (\partial b/\partial x)_0 = 0$ and $(\partial c/\partial x)_0 + (\partial d/\partial x)_0 = 0$; (4) for i_{RP}^{3}, $b_0 = c_0 = e_0 = 0$, $(\partial a/\partial x)_0 + (\partial b/\partial x)_0 = 0$, and $(\partial c/\partial x)_0 + (\partial d/\partial x)_0 = 0$. From the simulated limiting currents obtained for different values of the deligation rate constant k_1, the working curves illustrated in Figures7 and 8 were constructed. Since the analyzed current ratios depended also on time parameters t_p and $\tau = t_g + t_p$, three sets of working curves were simulated to match the time ratios used in the experiments. [Note that Feldberg's results of single-step chronoamperometry are equivalent to i_{NP}/i_{NP}^{a} used here, and the agreement is within ±1%.] With bis(arene)iron dications, the currents at five potential regions were simulated, viz. the limiting plateaus of the first NP wave (i_{NP}) and wave C (i_{NP}^{C}) (see Figures 3 and 7) as well as i_{DC}, i_1, and i_3 for the limiting currents of RP waves (see Figures 4, 6, and 8).

Acknowledgment. We thank the National Science Foundation, the R. A. Welch Foundation, and the Texas Advanced Research Program for financial support. Z.J.K. thanks the University of Warsaw for a leave of absence.

(35) Gagne, R. R.; Koval, C. A.; Lisensky, G. C. *Inorg. Chem.* **1980**, *19*, 2854.
(36) Gritzner, G.; Kuta, J. *J. Pure Appl. Chem.* **1984**, *56*, 461.
(37) Feldberg, S. W. In *Electroanalytical Chemistry*; Bard, A. J., Ed.; Marcel Dekker: New York, 1965; Vol. 3, p 199.
(38) Britz, D. *Digitial Simulation in Electrochemistry*; Springer: Berlin, 1985.